ADAPTIVE OPTICS PHOTOMETRY AND ASTROMETRY OF BINARY STARS. III. A FAINT COMPANION SEARCH OF O-STAR SYSTEMS*

NILS H. TURNER[1], THEO A. TEN BRUMMELAAR[1], LEWIS C. ROBERTS[2], BRIAN D. MASON[3], WILLIAM I. HARTKOPF[3], AND DOUGLAS R. GIES[4]

[1] Center for High Angular Resolution Astronomy, Georgia State University, The CHARA Array, Mount Wilson, CA 91023, USA; nils@chara-array.org, theo@chara-array.org

[2] The Boeing Company, 535 Lipoa Pkwy, Ste 200 Kihei HI 96753, USA[5]; lewis.c.roberts@jpl.nasa.gov

[3] United States Naval Observatory, Department of Astrometry, Washington DC, USA; bdm@usno.navy.mil, wih@usno.navy.mil

[4] Center for High Angular Resolution Astronomy, Department of Physics and Astronomy, Georgia State University, P.O. Box 4106, Atlanta, GA 30302-4106, USA; gies@chara.gsu.edu

ABSTRACT

We present the results of an adaptive optics survey for faint companions among Galactic O-type star systems (with $V \lesssim 8$) using the Advanced Electro-Optical System (AEOS) 3.6 m telescope on Haleakala. We surveyed these O-star systems in the I-band, typically being able to detect a companion with a magnitude difference of $\triangle m_I \lesssim 6$ in the projected separation range $0''.5 < \rho < 1''.0$, and $\triangle m_I \lesssim 9.5$ in the range $1''.0 < \rho < 5''.0$. In the course of the survey, we discovered 40 new companions among 31 of the 116 objects examined and made astrometric and differential magnitude measurements of 24 additional known pairs, several of them being confirmation detections. We present new astrometric orbits for two binaries, BU 1032AB (WDS 05387−0236; σ Ori AB) and SEE 322 (WDS 17158−3344; HD 155889AB). We lack magnitude differences for other filter bands, so it is difficult to determine physical from line-of-sight companions, but we present empirical arguments for the limiting magnitude difference where field contamination is significant.

Key words: binaries: close – binaries: general – instrumentation: adaptive optics – stars: early-type – techniques: high angular resolution

Online-only material: extended figure set

1. INTRODUCTION

Binary star systems are frequently the only source for the fundamental determination of the most basic property of a star, its mass. The masses of a sample of stars, when determined with sufficient accuracy, serve as crucial tests of our theoretical understanding of stellar formation, structure, and evolution. By combining information from the angular orbit projected on the sky (or from a light curve in the case of an eclipsing system) with the spectroscopic orbit, one can determine the distance and masses of the individual stars. In the case of the most massive stars, accurate masses are even more important, not only because massive stars are relatively rare, but because these stars (initial masses $> 20 M_\odot$) play critical roles in galaxies. Massive stars serve as signposts of star formation in galaxies (Massey et al. 1995). Current theory suggests that high-mass stars are born in loosely bound star clusters which disperse after a few Myr. These birth conditions suggest that high-mass stars might often have companions as, for example, found around γ^2 Velorum (Pozzo et al. 2000). Some of these could be very close and gravitationally bound to the O star, which is suggested by the prevalence of binary and triple systems among young O stars (Mason et al. 1998).

Mason et al. (1998) performed a speckle interferometry survey of Galactic O-type stars for close companions, specifically looking for differences in the multiplicity frequencies amongst the cluster, field, and runaway O-type star populations, as well as the distribution of orbital periods. They did their survey in the V-band using speckle interferometry, which is sensitive to the detection of a companion if the projected separation is in the range $0''.035 < \rho < 1''.5$ and the magnitude difference $\triangle m_V < 3$. Our survey is in the I-band (which will slightly emphasize redder companions) and extends the dynamic range of their work. Due to the availability of only one photometric band for this survey, we are unable to determine physical associations for the new companions with any certainty, and we can only address the likelihood that perhaps some of the companions are gravitationally bound. The results presented here invite further investigation into the O stars and their potential to shed light on star-formation processes.

2. OBSERVATIONS

The data were taken using the adaptive optics (AO) system and Visible Imager (VisIm) camera of the Advanced Electro-Optical System (AEOS) 3.6 m telescope at the Maui Space Surveillance System, located on Haleakala. The data were collected during four separate observing runs between 2001 February and 2002 September. In addition to the dedicated observing runs, some observations were taken as part of a queue-scheduled observation program between 2001 May and 2005 November.

2.1. AEOS Telescope and Adaptive Optics System

The AEOS telescope is an altitude–azimuth (alt-az) design. While the telescope is very flexible and supports several different optical configurations (Roberts & Neyman 2002), of interest here is the Cassegrain configuration which feeds a 726 m focal

length, $f/200$ beam (with a field of view (FOV) of 61″9) through a Nasmyth port coudé path to a fold flat below the telescope which directs the beam onto a custom optical table that supports the main components of the AO system. For this project, the short-wavelength light (400–700 nm) is sent to the wavefront sensor (WFS) and tracker camera beam trains, while the 700 nm–5 μm light is sent to the VisIm, which is used as the science detector.

The heart of the AO system is a Shack–Hartmann WFS driving a 941-actuator Xinetics deformable mirror (DM) with a stroke of ±4 μm. Optics inside the WFS produce a pupil image on a Hartmann lens array. Each generated Hartmann spot is then imaged onto a 4×4 group of pixels on the WFS CCD. These pixel values can be used directly or binned (for higher throughput) to generate the wavefront slopes. The WFS CCD is a Lincoln Labs frame-transfer device with 16 output ports, capable of frame rates of 0.2–2.5 kHz. The wavefront slopes are calculated from the Hartmann spot values by means of many digital signal processors working in parallel, feeding these data to a system which reconstructs the wavefront, taking into account alt-az-induced image rotation and WFS-to-DM-actuator mapping artifacts.

The VisIm camera is described in detail in Roberts & Neyman (2002). In short, it operates from 700 to 1050 nm; is equipped with an atmospheric dispersion corrector; has a two-mode image derotator (zenith at a fixed position in the image or celestial north at a fixed position in the image); and, for this project, has a 10″ FOV (0″020 pixel^{-1}). The detector is a 512×512 pixel EEV CCD with a dark current of 22 e^{-} pixel^{-1} s^{-1} (at $-40°$ C) and a read noise of 12 e^{-} rms. The camera output is digitized to 12 bits with 10 e^{-} per digital number.

2.2. Object Selection

The object list started out as all the components in the 228 systems listed in Mason et al. (1998). They were then culled for the effective magnitude limit of the AEOS AO system (about $m_V = 8$), and for the declination limit of acceptable AO correction (objects that at some time during the year get above 30° elevation at Haleakala, i.e., a declination greater than about $-45°$). This reduced the list to 164 objects. We added seven more targets from the Galactic O Star Catalog[6] (Maíz-Apellániz et al. 2004) that are within our adopted magnitude and declination limits. We actually observed, at least once, 116 of the 171 objects in our list. These observations are fairly consistently distributed among the three O-star populations, sampling 63% of the cluster membership stars, 78% of the field stars, and 88% of the runaway stars in our list of potential targets.

2.3. Data Collection and Reduction

Since VisIm is only a 12-bit camera, a stellar image can overflow the digitizer in a rather short exposure time. If the frame saturates, then it is omitted from the final image. Frequently, this saturated frame will represent a period of particularly good seeing. In order to keep as many of these "good seeing" frames as possible, we set the exposure time such that the average peak value was about 75% of the full-well depth. We then built up the signal-to-noise ratio by taking many frames, then weighting and summing them. Figure 1 shows the effect of this summing on the detectable magnitude difference for 1, 10, 50, 100, 250, and 1000 frame(s). On the basis of this plot, we aimed to take at least
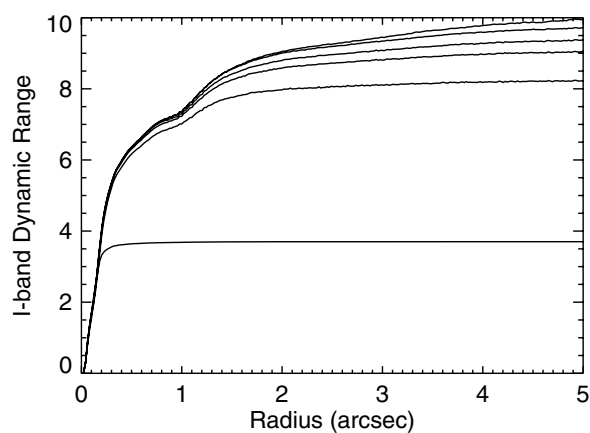
---
[6] http://www-int.stsci.edu/~jmaiz/research/GOS/GOSmain.html.

Figure 1. Assuming that a Gaussian-shaped peak, 3σ detection above background constitutes a positive detection of a companion, this plot shows the rough dynamic range of the AEOS AO system as a function of radius for different numbers of summed images. From top to bottom, the curves represent the results of 1000, 250, 100, 50, 10, and 1 summed frame(s). The "shelf," most apparent in the upper curves from about 0.7–1 arcsec in radius, is due to AO system artifacts.

1000 frames of each object, although time constraints, weather, and object brightness occasionally limited us to a lower-frame count.

The VisIm is a frame-transfer camera and is therefore unable to take a bias frame. To compensate, a bias frame was created by taking many dark exposures at a variety of exposure times ranging from 10 ms to several minutes. A linear fit was made to the signal from each pixel as a function of exposure time; the y-intercepts became the bias frame while the slopes became the dark frame. Prior to 2005, flat-field frames were created using the twilight sky to evenly illuminate the VisIm detector. Roberts (2001) found that sky flat-field frames varied at about the 1% level, so after 2005, flat-field frames were generated using an internal calibration sphere; this lowered the frame-to-frame variation below the 0.01% level. From this point, all data frames were debiased, dark subtracted, and flat fielded in the conventional way.

For a given sequence of data frames, a weighted shift-and-add algorithm was used to create the final image. The weighted shift-and-add algorithm (ten Brummelaar et al. 1998) is a modification of the traditional image-stacking algorithm that takes seeing conditions in each individual frame into account. Frames with higher peak values (which represent better seeing) influence the final image (by means of weighting) more than frames with lower peak values.

The fitting algorithm is described in detail in ten Brummelaar et al. (1996, 2000). In short, the point-spread function (PSF) used to represent the system performance is that of the primary star in the image, with a few modifications; near the primary, the PSF is a pixel-for-pixel table of numbers, while farther out the PSF is a radially-symmetric series of values. This PSF is fitted to the primary and secondary components and iterated until the intensity ratio converges.

2.4. Detection Sensitivity

Figure 1 only gives a qualitative sense of the companion detection sensitivity of the system. Cross comparisons of the reduced images, especially of the same object taken on different nights, show different detection limits. This is primarily due to variations in AO performance which is primarily attributed
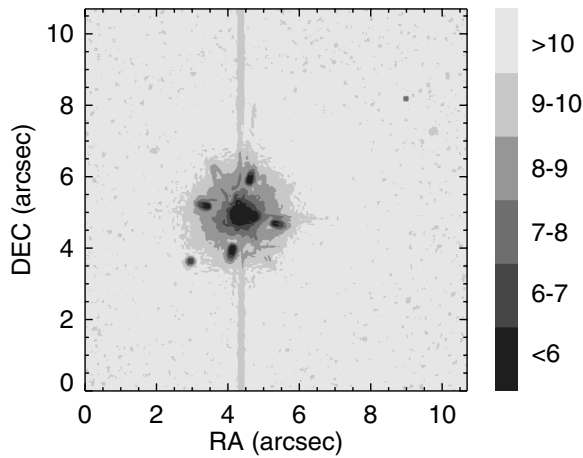
Figure 2. A sample dynamic range map (in this case, HD 34656, taken Bess. year 2003.7360). The gradient map on the right shows the 5σ detection limit for a given pixel of the image in magnitudes. There are several artifacts in this image which lower the dynamic range. The largest is the vertical line, which is an artifact of the shutter-less frame transfer process. There are also four waffle spots caused by the Fried geometry of the WFS. There are also hints of the diffraction pattern caused by the secondary mirror support spiders. These all increase the difficulty of finding any companions that coincide with these artifacts.

(An extended figure set is available in the online journal.)

to variations in the atmospheric turbulence profile. In order to quantify the sensitivity of the reduced images, we have created a variation of the "dynamic range map" technique described in Hinkley et al. (2007) which defines the dynamic range of a given position in a 2D image as the faintest companion detectable at that position to the 5σ level. In our version, we construct a map the same size as each reduced image. The intensity level of each pixel in the map is set to five times the root mean square (rms) intensity variation across a patch centered on the corresponding pixel in the original image. The patch is a square with lengths equal to the FWHM of the original image. This produces the dynamic range map in intensity terms, which are then converted to magnitudes.

Figure Set 2 shows the results of this technique applied to all of the images generated in this survey. It is apparent from the sample figure that the detection threshold for a companion is highly spatially variant. The dynamic range increases with increasing radius from the central star. There are several artifacts in this image which lower the dynamic range. The largest is the vertical line, which is an artifact of the shutter-less frame-transfer process. There are also four waffle spots caused by the Fried geometry of the WFS (Makidon et al. 2005). There are also hints of the diffraction pattern caused by the secondary mirror support spiders. As the AO system performance decreases, the FWHM of the PSF will increase, which increases the area over which the central PSF causes confusion. In addition, it also widens the companion's PSF, lowering the contrast between the two and decreasing the detection rate. After 2003, the waffle spots were greatly reduced when new reconstructors were put in place to filter out the unsensed waffle modes.

These maps have several purposes. For those objects with multiple observations where companions are seen in some but not all of the data, changes in the dynamic range can help explain the reasons for these discrepancies. They also illustrate the limitations of the data, showing where it is almost impossible to find faint companions. This is often useful when trying to detect known long-period spectroscopic companions.

3. RESULTS

3.1. New Pairs and New Measures

Table 1 lists the 40 new and 24 known pairs detected in the survey. Four of the new companions (HD 17505, HD 37468, HD 193793, and HD 217086) are in systems with previously known components in the AEOS FOV. The remainder are new companions in systems not previously known to be multiple (at least in the AEOS FOV). The table has nine columns which summarize the information gleaned from the measurements: Column 1 lists the Washington Double Star (WDS) identifier, Columns 2 and 3 identify the object by HD and *Hipparcos* number, and Column 4 gives the discoverer designation (TRN for new pairs). Circumstances of the observation are given in Columns 5–8. Column 5 gives the Besselian epoch of the start of the observation, Columns 6 and 7 give the position angle (P.A.) (in degrees, where north is $0°$ and east is $90°$) and separation (in seconds of arc) between the primary (the survey star—the brightest star in the image) and the detected component. Note that for many of the objects, the P.A. is missing or ambiguous. The VisIm derotator is usually in one of the two modes, one which keeps zenith up in the image, and one which keeps north up in the image. In the observations with more than one or a missing P.A., the state of the derotator was unknown, leaving the orientation of the image on the sky unknown. However, in some cases, the position of a known pair resolves the ambiguity while for the rest, new observations will be required. Column 8 gives the magnitude difference at the I-band between the primary and the detected component. Finally, Column 9 lists the spectroscopic status. Given the separations detected here, none of the short period spectroscopic pairs is expected to be detected. However, listing the spectroscopic binaries helps to form the complete multiplicity picture. The indicator in this table is V (velocity variable) if one or more close spectroscopic companions is indicated or C (velocity constant) if radial velocity work indicates no close companion. The spectroscopic reference is generally given in Mason et al. (1998).

The differential magnitude errors in Column 8 of Table 1 were generated from simulated binary data that we analyzed using the same fitting algorithm applied to the measured binary data. To generate the simulated binaries, we started by collecting all the single star images from this survey (see Table 4) and those of a duplicity survey B stars carried out contemporaneously (see Roberts et al. 2007, Table 2). We omitted single-star images where there were fewer than 250 frames used to make the final image. This exercise gave us 167 unique images with PSFs ranging from $0.''083$ to $0.''445$, with a decided emphasis on values less than $0.''2$. For each entry in Table 1, 167 simulated binaries were constructed using the magnitude difference in Column 8 and the pixel positions of the primary and secondary components in the main image. We then ran the fitting algorithm on each of these 167 simulated images for each table entry. We calculated the magnitude variance in two passes, the first to filter out outliers on the basis of the variance of the fitted pixel separation of the simulated binary (namely, any deviation greater than 1σ), and the second to use this reduced list of simulated fits to generate the final magnitude variance. In general, the number of outliers per table entry was less than 10. The errors quoted in Column 8 are the standard errors of these variances. Errors are not quoted for the separation (Column 7), but in all cases, the standard error is less than $0.''04$, usually less than $0.''005$. For errors in P.A. (Column 6), we adopt the values from Roberts et al. (2007), $±2°$ for separations less than $1''$, and $±1°$ for

Table 1
Survey Measurements

WDS (1)	HD (2)	HIP (3)	Discoverer designation (4)			Epoch (BY) (5)	P.A. (°) (6)	Separation (″) (7)	Δm_I (mag) (8)	Spectroscopic status[c] (9)
00061+6341	108	505	TRN	7		2001.7450	5Z/176N[a]	3.24	9.47 ± 0.26	C
00177+5126	1337	1415	TRN	8		2001.7341	22Z/186N[a]	2.75	9.30 ± 0.47	V
02158+5600	13745	10541	TRN	9		2004.7924	29	4.55	10.04 ± 0.67	V
02229+4129	14633	11099	TRN	10		2001.7451	97Z/214N[a]	2.18	10.31 ± 0.61	V
02327+6127	15558	11832	TRN	11	AF	2001.7450	261	4.45	6.59 ± 0.19	V
						2002.6845	261	4.48	6.38 ± 0.40	
						2005.6962	262	4.44	6.42 ± 0.30	
			TRN	11	AG	2001.7450	221	2.99	9.94 ± 0.35	
			TRN	11	AH	2001.7450	211	5.79	11.03 ± 0.86	
02407+6117	16429	12495	TRN	12	AD	2005.6963	112	2.94	7.39 ± 0.22	V
02511+6025	17505	13296	STF	306	AB	2001.7450	91	2.09	1.71 ± 0.26	V
						2002.6845	89	2.11	1.71 ± 0.37	
						2004.9648	92	2.10	1.64 ± 0.37	
			TRN	13	AH	2001.7450	142	4.59	6.72 ± 0.21	
						2002.6845	140	4.62	7.01 ± 0.27	
						2004.9648	143	4.59	7.15 ± 0.22	
02594+6034	18326	13924	TRN	14		2001.7451	223Z/353N[a]	2.38	7.45 ± 0.46	V
03141+5934	19820	15063	TRN	15		2001.7452	81Z/209N[a]	2.81	10.37 ± 0.42	V
03556+5238	24431	18370	HDS	494		2001.7455	176	0.71	2.86 ± 0.35	C
03590+3548	24912	18614	TRN	16		2001.7342	141Z/236N[a]	2.40	9.81 ± 1.16	C
05163+3419	34078	24575	TRN	17	Aa	2004.7873	171	0.35	4.97 ± 0.51	C
05207+3726	34656	24957	TRN	18	Aa	2002.7257	279	0.35	3.77 ± 0.33	C
						2003.7360	280	0.35	4.09 ± 1.10	
						2003.8917	280	0.34	4.13 ± 0.84	
			TRN	18	AB	2002.7257	48	1.88	6.98 ± 0.24	
						2003.7360	47	1.90	6.94 ± 0.25	
						2003.8917	47	1.89	7.28 ± 0.43	
			TRN	18	AC	2003.7360	126	2.96	10.57 ± 0.68	
			TRN	18	AD	2003.7360	247	5.75	10.39 ± 0.42	
05297+3523	35921	25733	HU	217		2004.7873	253	0.61	2.23 ± 0.31	V
05351+0956	36861		STF	738	AB	2001.7428	297Z/356N[a,b]	4.25	2.29 ± 0.16	C
						2001.7456	41	4.23	2.04 ± 0.15	
05353−0523	37022	26221	STF	748	Ca,F	2001.7456	118	4.39	4.89 ± 1.06	V
						2003.0045	120	4.46	4.73 ± 0.19	
05354−0525	37041	26235	CHR	249	Aa	2004.8666	292	0.39	2.97 ± 0.72	V
05387−0236	37468	26549	BU	1032	AB	2001.7456	106	0.24	1.22 ± 2.15	V
			TRN	19	AF	2001.7456	18	3.13	8.07 ± 0.33	
05407−0157	37742		STF	774	Aa-B	2001.7455	160	2.36	2.24 ± 0.89	C
06319+0457	46150	31130	GAN	3	AB	2001.0989	284	3.47	4.87 ± 0.13	C
06322+0450	46223	31149	TRN	20		2001.8661	314Z/264N[a]	0.46	4.37 ± 0.17	C
06364+0605	46966	31567	TRN	21		2002.8023	210	3.19	9.97 ± 0.63	C
06374+0608	47129	31646	TRN	22	AB	2002.2404	240	1.15	5.10 ± 0.43	V
						2005.0144	251	1.16	4.94 ± 0.22	
			TRN	22	AC	2005.0144	203	0.78	5.14 ± 0.22	
06386+0137	47432	31766	TRN	23		2005.0134	206	0.78	4.95 ± 1.31	C
06410+0954	47839	31978	STF	950	Aa-B	2001.7457	202	2.88	3.31 ± 2.11	V
06427+0143	48279	32137	STF	956	AB	2004.0478	199	6.63	2.57 ± 0.39	C
08392−4025	73882	42433	B	1623		2004.1190	256	0.65	1.25 ± 0.77	V
16550−4109	152408	82775	I	576		2001.4030	260Z/261N[a]	5.30	5.67 ± 0.92	C
17065−3527	154368	83706	B	894		2002.6730	357	2.57	6.28 ± 0.54	V
17158−3344	155889	84444	SEE	322		2003.6041	285	0.19	0.68 ± 2.59	C
17175−2746	156212	84588	TRN	24	AB	2001.4959	206Z/204N[a]	4.04	8.05 ± 0.39	C
			TRN	24	AC	2001.4959	145Z/144N[a]	7.31	7.40 ± 0.24	
17347−3235	159176	86011	HDS	2480	Ab	2003.3280	59	0.70	3.14 ± 0.47	V
17595−3601	163758		TRN	25		2001.4960	107Z/ 93N[a]	1.70	8.05 ± 0.33	C
18024−2302	164492	88333	TRN	26	AH	2002.4516	342	1.48	5.12 ± 0.23	V
18026−2415	164536		RST	3149	AB	2002.4627	62	1.65	4.49 ± 12[d]	C
18061−2412	165246		B	376		2002.4819	98	1.90	3.68 ± 0.47	V
18152−2023	167263		BU	286	AB	2005.6545	216	5.93	5.62 ± 0.98	V
18181−1215	167971	89681	TRN	27		2001.7447	80Z/ 39N[a]	4.70	8.12 ± 0.32	V
20035+3601	190429	98753	STF	2624	Aa-B	2001.7337	172	1.92	0.84 ± 0.95	C
20181+4044	193322	100069	STF	2666	Aa-B	2001.6683	244	2.69	2.51 ± 0.12	V
						2001.7364	243	2.67	2.11 ± 0.26	

Table 1
(Continued)

WDS (1)	HD (2)	HIP (3)	Discoverer designation (4)		Epoch (BY) (5)	P.A. (°) (6)	Separation (″) (7)	Δm_I (mag) (8)	Spectroscopic status[c] (9)
20191+3916	193514	100173	TRN 28	AB	2001.7367	78	4.75	5.80 ± 0.17	C
					2002.6730	79	4.79	6.18 ± 0.25	
			TRN 28	AC	2001.7367	157	3.20	7.23 ± 0.28	
					2002.6730	158	3.22	7.44 ± 0.16	
20205+4351	193793	100287	BU 1207	AB	2001.3400	209	4.77	8.44 ± 0.31	V
					2001.7337	209	4.77	6.75 ± 0.28	
					2001.7363	209	4.77	6.75 ± 12[d]	
					2001.7447	. . .[b]	4.79	6.43 ± 0.53	
					2002.6731	210	4.81	6.58 ± 0.13	
					2002.6731	210	4.81	6.93 ± 0.12	
			TRN 29	AC	2001.7363	202	2.29	9.62 ± 0.35	
					2001.7447	. . .[b]	3.23	9.32 ± 0.38	
20566+4455	199579	103371	TRN 30		2001.7338	30Z/205N[a]	3.76	9.79 ± 0.29	V
21079+3324	201345	104316	TRN 31		2001.7367	342Z/218N[a]	7.38	9.31 ± 0.47	C
21185+4357	203064	105186	TRN 32		2001.7337	81Z/219N[a]	3.84	9.48 ± 0.29	C
21390+5729	206267	106886	BU 1143	AB	2001.7338	317	1.78	5.65 ± 0.21	V
21449+6228	207198	107374	TRN 33	AC	2001.7364	75Z/207N[a]	2.96	10.43 ± 0.52	C
22021+5800	209481	108772	TRN 34		2001.7341	358Z/208N[a]	2.75	9.92 ± 0.46	V
22051+6217	209975	109017	TRN 35	AD	2001.7367	341Z/171N[a]	4.14	9.98 ± 0.44	C
			TRN 35	AE	2001.7367	344Z/175N[a]	3.79	10.03 ± 0.37	
22393+3903	214680	111841	TRN 36	AC	2001.7339	85Z/222N[a]	3.56	9.94 ± 0.45	C
22568+6244	217086	113306	MLR 266	AB	2001.7369	353	2.79	3.41 ± 0.27	C
					2002.6843	354	2.83	3.34 ± 0.48	
					2004.7598	354	2.78	3.79 ± 0.58	
			TRN 37	AC	2001.7369	164	3.15	7.14 ± 0.29	
					2002.6843	165	3.17	6.79 ± 12[d]	
					2004.7598	165	3.12	7.03 ± 0.34	

Notes.

[a] Image derotator in an unknown state: Z = zenith up and N = north up. Confirmation of the pair will clear up this residual ambiguity.

[b] Image derotator in an unknown state. Neither zenith up or north up match coordinates of known object in field.

[c] Codes are V, one or more additional spectroscopic companions indicated or C, radial velocity constant.

[d] This is a lower limit for the errors, the actual errors are typically much larger.

Table 2
Orbital Elements

WDS designation $\alpha\delta$ (2000)	Discoverer designation		Period P (yr)	Semimajor axis a (″)	Inclination i (°)	Longitude of node Ω (°)	Epoch of periastron T_o (yr)	Eccentricity e	Longitude of periastron ω (°)
05387−0236	BU 1032	AB	156.7 ±3.0	0.2662 ±0.0021	159.7 ±3.7	121.7 ±9.6	1999.5 ±10.2	0.0515 ±0.0080	8.7 ±16.9
05387−0236	BU 1032	AB[a]	155.3 ±7.5	0.2642 ±0.0052	160.4 ±7.2	136. ±25.	1997. ±24.	0.051 ±0.015	18. ±37.
17158−3344	SEE 322		536.	0.35	111.	167.	1870.	0.64	109.

Note. [a] Elements from (Hartkopf et al. 1996).

separations greater than 1″. Two effects lead to this uncertainty, the clocking calibration of the dove prism in the derotator, and the slight natural image rotation during the frame collection sequence when the derotator is in the fixed zenith position mode.

3.1.1. Notes to Pairs

Here we discuss the various binary systems in Table 1 by WDS identifier and discovery designation. In the cases of the stars classified as runaways, it is unlikely that the detected companion is physical (see Section 4).

02229+4129 = TRN 10. This is a runaway star with a close, low-luminosity companion (Boyajian et al. 2005).

02407+6117 = TRN 12AD. The A component is a spectroscopic triple (McSwain 2003).

02511+6025 = TRN 13AH. The A component of HD 17505 is a spectroscopic triple (Hillwig et al. 2006). It is uncertain if the new component (AH, $\rho \sim 4\farcs6$) and the known pair of Table 1 (STF 306AB) are both gravitationally bound. If STF

306AB is indeed gravitationally bound, Hillwig et al. (2006) estimate it to have a period of 27,000 years.

03556+5238 = HDS 494. The $\triangle m$ was probably a little too large for Mason et al. (1998) to detect this pair, but it was detected in later speckle observations by Mason et al. (2001a).

03590+3548 = TRN 16. Classified as a runaway star in Gies & Bolton (1986).

05163+3419 = TRN 17Aa. Classified as a runaway star in Gies & Bolton (1986). SEI 136AB ($\rho \sim 8\rlap{.}{''}8$, $\triangle m \sim 3.3$, just outside the FOV) is a likely optical pair, with the B component not physically associated with this close double.

05207+3726 = TRN 18. One new close pair and three wide pairs are found here. The close one is designated Aa while the wider pairs are designated AB, AC, and AD. The known pair SEI 201 ($\rho \sim 24\rlap{.}{''}7$, $\triangle m \sim 5.9$) is outside the FOV and has been designated AE.

05297+3523 = HU 217. This known, relatively close, pair has been measured since 1900. The P.A. has only changed by $4°$ over this time span.

05353−0523 = STF 748Ca,F. The primary is θ^1 Ori C, the most massive star in the Orion Trapezium. It has a closer companion discovered by speckle methods (Kraus et al. 2007).

05354−0525 = CHR 249Aa. Perryman & ESA (1997) measured a $\triangle H_p$ of 3.23. Fabricius & Makarov (2000) found $\triangle B_T = 4.37 \pm 0.02$ and $\triangle V_T = 3.21 \pm 0.01$.

05387−0236 = TRN 19AF. The new component (AF) is at a separation nicely nestled between BU 1032AB and STF 762AC, at a value which would be consistent with a hierarchical arrangement. The new TRN 19AF component is much brighter in the mid-infrared where it was first discovered (van Loon & Oliveira 2003) and it is probably a low-mass K-star surrounded by a circumstellar disk (Caballero 2007). See Section 3.1.3 below for a discussion of the orbit of BU 1032AB.

05407−0157 = STF 774Aa-B. This pair has an orbit (Hopmann 1967) with residuals of O−C = $-5°$ and $-0\rlap{.}{''}03$ in P.A. and separation. However, the orbit is classified as "indeterminate" (grade 5) in the 6th Catalog of Orbits of Visual Binary Stars,[6] so these residuals are not indicative of measurement quality. While the total number of measures has increased by about 50% since this orbit was published, the initial elements are of such low quality that even at this point any sort of improvement above "indeterminate" subjective quality is not yet possible. Some of the scatter in the residuals may be due to the presence of a closer companion to ζ Ori A found by interferometry (Hummel et al. 2000).

06319+0457 = GAN 3AB. The measure agrees with earlier published data quite well and indicates that the measure made in 1928 (Silbernagel 1931) is probably erroneous.

06410+0954 = STF 950Aa-B. This pair has only been changed by $\sim 9°$ and $0\rlap{.}{''}2$ since it was first resolved by Struve in 1825 (Struve 1837).

16550−4109 = I 576. I 576 has not been measured since 1934 (Wallenquist 1934), so identification of this pair with that of Innes is uncertain.

17065−3527 = B 894. This binary, unconfirmed since its first resolution by van den Bos (1928), has closed slightly.

17158−3344 = SEE 322. This pair has shown noticeable Keplerian motion, completing about $70°$ of orbital revolution since discovery (See 1898). See Section 3.1.3 below for a discussion of the orbit.
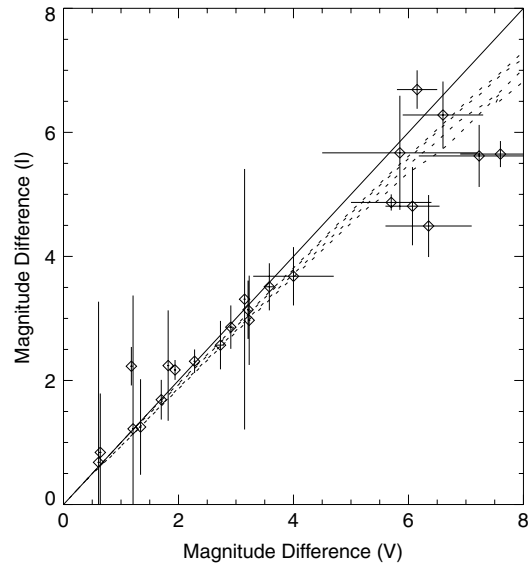
7 http://ad.usno.navy.mil/wds/orb6.html.

Figure 3. *V*-band magnitude differences from the WDS vs. *I*-band values from AO. The solid line indicates a 1:1 relation between $\triangle V$ and $\triangle I$, while the various dotted curves illustrate the expected trend assuming main-sequence primaries of types O3, O5, O8, and B0 (from top to bottom, respectively) and a range of later spectral-type secondaries.

17347−3235 = HDS 2480Ab. The pairs, ISO 5 and HJ 4962 should have been seen as well. ISO 5 was probably missed due to the corrected FWHM. HJ 4962 was probably just out of the field.

18024−2302 = TRN 26AH. While this pair may be physical, the known double H N 40 almost certainly is not.

18026−2415 = RST 3149AB. This pair has been seen only twice since 1935. The occultation pair of Africano et al. (1975) was not seen.

18061−2412 = B 376. Unconfirmed since its discovery in 1927 (van den Bos 1928). The A component is an eclipsing binary with a 4.6 d period (Otero 2007).

20035+3601 = STF 2624Aa-B. The close pair, MCA 59Aa, which is notoriously difficult to detect, was not seen here.

20181+4044 = STF 2666Aa-B. The close speckle pair CHR 96Aa was not recovered.

20205+4351 = TRN 29AC. It is unclear whether there are two new components or a nearby optical pair with a large relative proper motion detected at two different positions.

21390+5729 = BU 1143AB. The close Aa pair (MIU 2) was not recovered, although it may have been too close.

21449+6228 = TRN 33AC. The visual pair, MLR 16, would have been much too wide ($17\rlap{.}{''}6$) to detect here.

22393+3903 = TRN 36AC. The visual binary, S 813, at ~ 1 arcmin of separation is much too wide to detect here.

22568+6244 = TRN 37AC. It is hard to imagine a geometry where both this pair and MLR 266 would be dynamically stable. More than likely one (or both) are optical.

3.1.2. Comparison of V- and I-Band Magnitude Differences

Among the O-star primaries listed in the WDS, we may estimate the companion spectral type from the magnitude difference $\triangle V$ for those with small magnitude differences. As the magnitude difference gets larger, the uncertainty in the companion spectral type increases. However, the situation improves with the availability of magnitude differences for two filters. We compare the *V*-band magnitude differences from the WDS with the *I*-band values we determined by AO. The result is shown in Figure 3. Error bars for the visual data were based
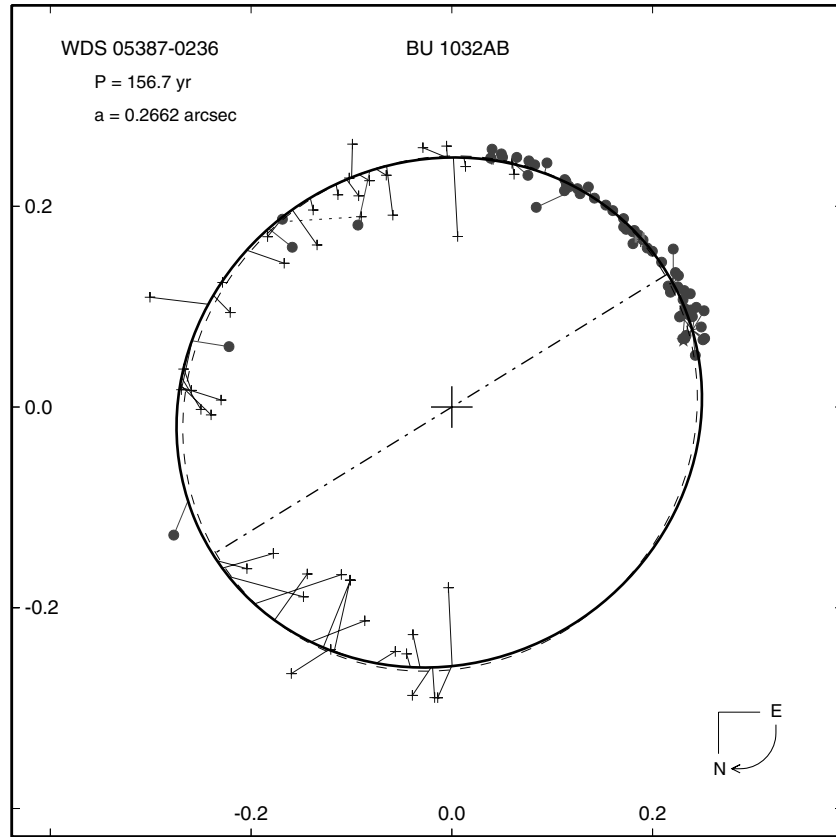
Figure 4. Relative visual orbit of BU 1032; the *x* and *y* scales are in arcseconds. The solid curve represents the newly determined orbit (Table 2). The dot-dashed line indicates the line of nodes. High-resolution measurements are shown as filled circles (speckle) or filled stars (AO). Visual measurements are denoted with plus signs. The orientation and direction of motion are indicated in the lower-right corner of the plot. The orbit of Hartkopf et al. (1996) is shown as a dashed curve, which matches the new orbit quite well.

Table 3
Future Ephemerides (BY) for BU 1032 and SEE 322

WDS designation α, δ (2000)	Discoverer designation		2008 θ (°) ρ ('')		2010 θ (°) ρ ('')		2012 θ (°) ρ ('')		2014 θ (°) ρ ('')		2016 θ (°) ρ ('')	
05387−0236	BU	1032 AB	93.0	0.249	88.0	0.249	83.1	0.248	78.1	0.247	73.1	0.246
17158−3344	SEE	322	281.7	0.184	280.4	0.184	279.0	0.183	277.7	0.183	276.3	0.183

on typical *Tycho-2* photometric errors when available (smaller-$\triangle m$ pairs), and on scatter among individual visual estimates for those (larger-$\triangle m$) systems with more than one such estimate. A rough average value of this scatter (0.7 mag) was used for systems with only one visual $\triangle m_V$ estimate. Mean $\triangle m_I$ values and error bars are given for systems with multiple observations. For systems with no *I*-band error estimate a default value of 0.5 mag was adopted.

This figure shows that $\triangle V \approx \triangle I$ for small magnitude differences, but $\triangle V$ increases more rapidly at larger values of $\triangle I$. This is as expected for our set of O-star targets: the components of small-$\triangle m$ systems are of similar spectral type, but the secondaries become later in spectral type—hence redder—as $\triangle m$ increases.

To determine the expected extent of this trend, absolute *V* and *I* magnitudes for main-sequence spectral types were extracted from Allen's Astrophysical Quantities (Cox 2001). Values of $\triangle V$ and $\triangle I$ were then determined, assuming primaries of spectral types O3, O5, O8, and B0 and secondaries covering a wide range of spectral types. The results, plotted as dotted lines in Figure 3, appear to be in good agreement with the trend seen

in these AO observations and are consistent with the assumption that the companions are physical.

3.1.3. Orbits of BU 1032 (σ Ori AB) and SEE 322 (HD 155889)

Worley (1990) provides guidelines as to when a collection of binary star measures merits the publication of a new orbit. Following these criteria, we determined that two systems, BU 1032 and SEE 322, deserved new orbital solutions. All available measures for these pairs were extracted from the WDS (Mason et al. 2001b) and individual measures were weighted following the precepts of Hartkopf et al. (2001). The orbital elements were determined with an iterative three-dimensional grid-search algorithm (Seymour et al. 2002). For these two pairs, orbital elements are provided in Table 2 and future ephemerides in Table 3. Elements from the Hartkopf et al. (1996) orbit for BU 1032 are provided for comparison. Due to the preliminary nature of the SEE 322 orbit, errors are not quoted. These orbits are illustrated in Figures 4 and 5.

Since the publication of the orbital elements of BU 1032 by Hartkopf et al. (1996), the number of measures has increased by about 35%, and while the prior orbit adequately fits these data, a
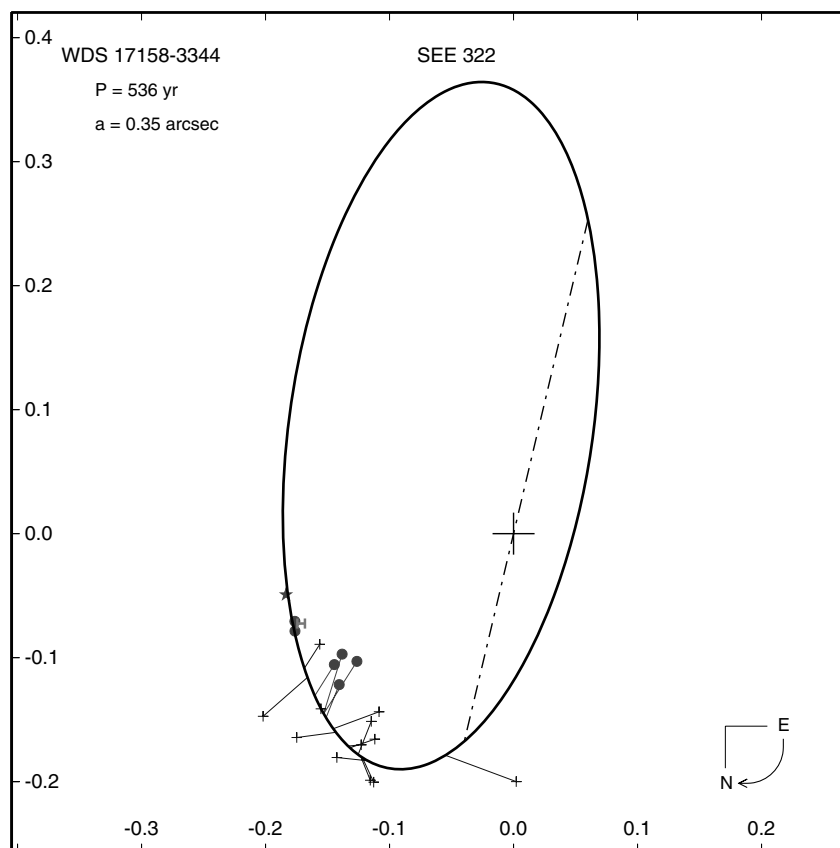
Figure 5. Relative visual orbit for SEE 322 in the same format as Figure 4. The **H** indicates the measure of *Hipparcos*.

new calculation at this time makes a significant improvement in the orbit quality, as illustrated by the decrease in formal errors for each of the elements. The distance and mass of the σ Ori AB system are discussed in a recent paper by Caballero (2008).

There is no previous determination of orbital elements for SEE 322. While the errors and residuals are large, the orbital solution looks promising, although it is still preliminary since only a limited portion of the orbit is covered by existing data. The total mass associated with this solution is very large (260 $M_\odot$ for a distance of 1.2 kpc; Mason et al. 1998), which may indicate that revisions are required in the assumed elements and distance, or that the system contains more than two stars.

3.2. Single-Star Detections

In addition to discovering new companions and measuring some parameters of previously known stars, we have a number of stars determined to be single under the specific observing conditions, AO system performance, and FOV. Table 4 lists these stars. In this table, the respective columns give the HD number, Hipparcos number, epoch of observation, FWHM of the corrected stellar PSF, and the V/C code for the spectroscopic binary status (see Section 3.1). A larger FWHM is indicative of poorer seeing, a dimmer primary, non-optimal AO system tuning, or some combination of these factors.

3.2.1. Notes to Unresolved Systems

HD 15137. This runaway star is a probable, single-lined spectroscopic binary (Boyajian et al. 2005).

HD 25638. The pair ES 2603 ($\rho \sim 6\farcs5$, $\triangle m \sim 6.0$) was not detected. It was probably just out of the FOV.

HD 30614. Classified as a runaway star in Gies & Bolton (1986).

HD 36879. This star is a runaway object according to its proper motion (Mdzinarishvili & Chargeishvili 2005).

HD 37042. The known components to this star are all far too wide for detection here. The star θ^2 Ori B is radial velocity variable according to Morrell & Levato (1991).

HD 37043. Iota Ori is a close speckle pair of great interest as, despite its very close separation, it was deemed optical in Gualandris et al. (2004). The speckle pair was last measured very close to the FWHM value, so it is possible that the component was just barely too close to be detected.

HD 37366. This star is a double-lined spectroscopic binary (Boyajian et al. 2007b).

HD 39680. Classified as a runaway star in Gies & Bolton (1986). The known pair, S 502, is much too wide (46$\farcs$1) for detection here.

HD 41161. The known pair, ES 1234AB, was too wide (10$\farcs$3) for detection here. Whether this pair is bound or not is not yet certain.

HD 45314. CHR 251 was last measured closer (54 mas) than the FWHM of the PSF of our observation. The A component is an Oe star and a probable velocity variable (Boyajian et al. 2007a).

HD 52266. This star is a probable single-lined spectroscopic binary (McSwain et al. 2007).

HD 54662. This star is a double-lined spectroscopic binary (Boyajian et al. 2007b).

HD 60848. This Oe star shows emission line variations but no evidence of significant velocity variability (Boyajian et al. 2007a).

Table 4
Single-Star FWHM measures

HD	HIP	Epoch (BY)	FWHM (″)	Spectroscopic statusa
14947	11394	2001.7455	0.12	C
15137	11473	2004.7923	0.18	V
25638	19272	2004.8665	0.12	C
30614	22783	2004.8665	0.12	C
36879	26272	2003.8944	0.11	C
37042		2004.8667	0.12	V
37043	26241	2001.7455	0.08	V
37366	26611	2005.0200	0.34	V
39680	27941	2002.2404	0.22	C
41161	28881	2001.8659	0.16	C
42088	29216	2001.8660	0.21	C
45314	30722	2001.0989	0.11	V
46149	31128	2001.8660	0.36	V
46966	31567	2002.2377	0.25	C
48099	32067	2002.2405	0.13	V
52266	33723	2001.9754	0.12	V
53975	34297	2005.0196	0.12	V
54662	34536	2002.0218	0.16	V
		2002.2404	0.12	
55879	34999	2005.0170	0.19	C
57061	35415	2004.0807	0.21	V
57682	35707	2001.9290	0.45	C
60848	37074	2001.0990	0.16	C
66811	39429	2004.0861	0.48	C
69648		2004.0451	0.26	...
75211	43125	2004.1432	0.23	...
75222	43158	2005.0197	0.49	C
93521	52849	2001.0992	0.19	C
148546	80829	2005.3482	0.28	C
149404	81305	2001.3893	0.12	V
149757	81377	2002.2243	0.22	C
151003	82121	2004.2590	0.23	V
151515	82366	2004.3384	1.93	C
152003		2001.3893	0.12	C
152219		2004.5265	0.22	V
152314		2001.4029	0.17	C
153919	83499	2003.5247	0.16	V
155806	84401	2002.6730	0.12	C
157857	85331	2002.2383	0.22	C
162978	87706	2001.7446	0.12	C
163758		2001.5179	0.17	C
163800	88040	2001.4960	0.13	...
		2001.5176	0.16	
163892	88085	2005.3404	0.21	V
164438	88297	2002.3204	0.16	...
164794	88469	2002.6729	0.10	V
164816		2001.6709	0.14	V
		2002.4817	0.11	
165052	88581	2001.6711	0.14	V
165319	88652	2001.6711	0.16	C
167771	89630	2002.4843	0.20	V
		2002.4950	0.19	
175876	93118	2001.7447	0.14	C
186980	97280	2001.7366	0.19	C
188001	97796	2001.7338	0.12	V
		2001.7447	0.17	
188209	97757	2004.7646	0.08	C
190864	98976	2001.7365	0.14	V
190918	99002	2001.7421	0.18	V
191612	99308	2001.7365	0.13	V
191978	99439	2002.6786	0.33	C
192281	99580	2001.7365	0.12	C
192639	99768	2001.7366	0.17	C
193443	100146	2001.7366	0.19	V

Table 4
(Continued)

HD	HIP	Epoch (BY)	FWHM (″)	Spectroscopic statusa
195592	101186	2005.6549	0.19	V
198846	102999	2005.3843	0.12	V
202124	104695	2005.6549	0.19	C
203064	105186	2001.7342	0.12	C
		2001.7448	0.12	
207538	107598	2005.7180	0.22	C
210809	109562	2001.7369	0.21	C
210839	109556	2001.7342	0.16	C
214680	111841	2001.7369	0.19	C
216898	113218	2001.7451	0.10	...
218915	114482	2004.7597	0.18	C

Note. a Codes are V, one or more additional spectro-
scopic companions indicated or C, radial velocity con-
stant.

HD 69648. Not included in the Mason et al. (1998) survey.

HD 163892. These data were taken using an 800–900 nm
filter.

HD 164794. This star is a probable long-period spectroscopic
binary (Rauw et al. 2002).

HD 167771. The known companion, RST 3170, last measured
in 1940 at 8″.3 (Rossiter 1955), would have been outside the FOV.

HD 175876. The known, probably optical, pair, HO 271,
would have been too wide to detect.

HD 191978. Not included in the Mason et al. (1998) survey.
The star shows no evidence of velocity variability (Abt et al.
1972).

HD 193443. The close pair, A 1425AB ($\rho \sim 0''.1$) may have
been too close to resolve, while the wider AC pair ($\rho \sim 9''.1$)
may have been outside the FOV.

HD 195592. This is a probable single-lined spectroscopic
binary (McSwain et al. 2007).

HD 216898. Not included in the Mason et al. (1998)
survey.

3.3. 2MASS Data Mining Confirmations

Searches were made for Two Micron All Sky Survey
(2MASS) (Cutri et al. 2003) companions to all stars on our
observing list, using Vizier and Aladin, as well as the "data
mining" technique of Wycoff et al. (2006). Results are given in
Table 5 and discussed below.

It should first be noted that the separation/△m regimes
covered by these two techniques have rather limited overlap.
The "plate scale" of the AO detector nominally limits us to
companions within $\sim 5''$ of the primary, although this outer
limit may extend to as wide as 7″.5, depending on orientation
of the pair relative to the detector, as well as slight off-center
placement of the primary.

In order to get an idea of the separation/△m limits of
2MASS, the point-source catalog was searched for sources
in the magnitude range $5.5 \leqslant J \leqslant 8.0$, corresponding to the
approximate 2MASS J-magnitude range for the AO targets in
this project. This yielded 99,656 sources. All sources within
$10''$ of these "primaries" were then extracted from the catalog,
yielding 9657 companions. A plot of separation versus △J
is shown in Figure 6. As seen in this figure, very few close
pairs are detected (only 17 pairs with separations in the range
$1'' < \rho < 2''$ and an additional 70 in the range $2'' < \rho < 3''$).
For the main body of companions, maximum △J increases to
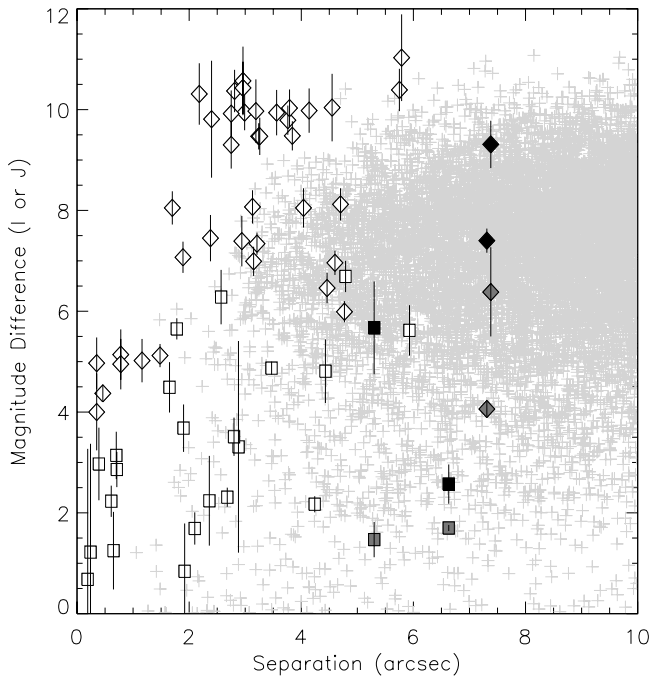
Figure 6. Magnitude difference versus separation from 2MASS and AO. AO observations are shown as squares (for previously-known pairs) or diamonds (for new pairs), with error bars plotted for the photometry only. The faint cloud of plus signs indicate all 2MASS pairs under $10''$ in separation, as described in the text. Two known and two new AO pairs were also found in the 2MASS data; these are shown as filled symbols, with 2MASS J-band magnitude differences in gray and AO magnitude differences in black. V-band magnitude differences for the two known pairs with AO and 2MASS data were very similar to the AO $\triangle m$ values, so are not plotted.

perhaps 6–6.5 mag at $3''$, 8–8.8 mag at $4''$, and 9.5–10 mag at $7''.5$.

AO Single Stars. A Vizier search of the regions around each of the AO single stars found only six 2MASS companions within $7''.5$ of their respective primaries. HD 25638 ($6''.2$), HD 52266 ($7''.1$), HD 151515 ($6''.2$), HD 152219 ($7''.2$), HD 163892 ($6''.4$), and HD 210809 ($5''.6$). A further check of their orientations showed that all of these companions fell either outside the observing window or so close to the edge of the field as to not be measurable. The companion to HD 25638 is known; see Section 3.2.1.

Known Pairs. A search of the regions around these primaries found six 2MASS companions within $7''.5$. Two of these (HD 48279 and 152408) correspond to known companions also measured by AO and are listed in Table 5, which lists relative astrometry and differential photometry in the 2MASS J, H, and K_S bands. The remaining four, including one known companion and three objects much wider than the known secondaries, all fall outside the AO observing window. Note that the companion to HD 152408 is very red ($\triangle m_I > \triangle m_{K_s}$), perhaps indicating that the companion still possesses a luminous disk (like the case of the IR-bright companion of σ Ori AB).

New Pairs. The search around these objects found five 2MASS companions within $7''.5$. Two of these (HD 156212 and 201345) correspond to the newly discovered AO companions and are listed in Table 5. The other three—two of which are known companions—are all wide.

4. DISCUSSION

Our AO survey of the O-stars has revealed a large number of new and generally faint companions. We show in Figure 7

the distribution of numbers of companions as a function of magnitude difference $\triangle I$ (in 1 mag bins), and the distribution peaks near $\triangle I = 10$ mag. It is certainly possible that some of these faint companions are low mass, gravitationally bound stars. For example, Hillenbrand (1997) made a deep I-band survey of the Orion cluster centered on the Orion Trapezium, and she found examples of still embedded pre-main-sequence stars with magnitude differences as large as $\triangle I = 15$ mag compared to the bright O-stars in the Trapezium. On the other hand, her survey also demonstrates that there will be many cluster stars that appear projected on the sky at positions near O-stars but are not orbitally bound to them.

We used the I-band star counts from Hillenbrand (1997) to model the possible confusion limit caused by nearby cluster stars that we might expect to find in our observations. The cumulative number distribution of stars brighter than I in her sample (1551 stars with measured I magnitudes) is well matched by a power law,

$$N(<I) = (0.063)\,10^{\gamma I}, \qquad (1)$$

where the exponent is $\gamma = 0.27$ (valid down to $I = 16$ mag). The total surface density of stars in the central part of cluster where the O-stars reside is $10^{5.4}$ stars per square degree (see Figure 4a in Hillenbrand 1997) or 1.9 stars per $10'' \times 10''$ FOV (= AEOS FOV). Thus, the cumulative distribution of cluster background stars per AEOS FOV is approximately given by

$$N(<I) = (7.8 \times 10^{-5})\,10^{\gamma I}. \qquad (2)$$

If we suppose that all O-stars have a color index of $V - I = -0.39$ (Wegner 1994), the extinction to Orion is approximately $A_I = 0.25$ (Hillenbrand 1997; Fitzpatrick 1999), and the distance to Orion is 470 pc (Hillenbrand 1997), then the numbers per AEOS FOV can be recast in terms of an O-star absolute magnitude M_V and magnitude difference $\triangle I$ as

$$N(<I) = (0.023)\,10^{\gamma(\triangle I + M_V)}. \qquad (3)$$

If we further assume that the same relationship holds for other O-stars in more distant clusters, then the number of cluster stars appearing in the FOV will scale as distance d squared. Let η represent the predicted number of cluster background stars per AEOS FOV. The relation between the limiting magnitude difference $\triangle I$ associated with η is then

$$\triangle I = 3.6 - \frac{2}{\gamma} \log d - M_V + \frac{1}{\gamma} \log \eta. \qquad (4)$$

Thus, we expect that background confusion with cluster stars will increase (smaller $\triangle I$) with increasing distance and with lower-luminosity O-stars.

We applied this relation to estimate a limiting $\triangle I$ for each cluster and the association star in our sample in order to separate the probable physical companions from the faint optical companions caused by background confusion. We used distances from Mason et al. (1998) and the spectral type—absolute magnitude calibration from Martins et al. (2005). The Orion cluster richness, extinction, and age may not be representative of the full sample of cluster O-stars in our survey, and so the normalization of the $\triangle I$ relation is somewhat uncertain. We note that large numbers of companions begin to appear near $\triangle I = 8$ mag (see Figure 7), and for typical O-star distances ($d = 1$ to 2 kpc) and magnitudes ($M_V = -4$ to -6) this corresponds
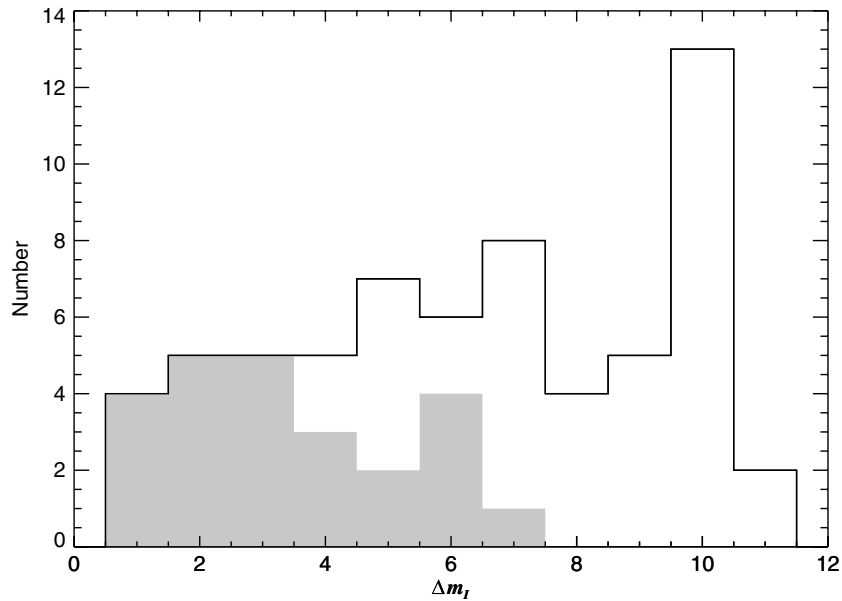
Figure 7. Number of companions vs. differential magnitude at *I*-band. Each bin represents a magnitude difference of 1 mag. The shaded region represents previously known companions while the solid line histogram shows the total number of companions (known plus new).

Table 5
Data Mining Results from 2MASS

Discoverer designation	HD	HIP	WDS	Epoch (BY)	P.A. (°)	Separation (″)	Δm_J (mag)	Δm_H (mag)	Δm_{K_s} (mag)
STF 956 AB	48279	32137	06427+0143	1999.87	194.8	6.55	1.70 ± 0.06	1.63 ± 0.03	1.56 ± 0.04
I 576	152408	82775	16550−4109	1999.36	264.2	4.72	1.47 ± 0.35	1.71 ± 0.58	1.25 ± 0.44
TRN 24 AC	156212	84588	17175−2746	1998.53	147.6	7.32	4.06	5.38 ± 0.14	4.24
TRN 31	201345	104316	21079+3324	1999.75	220.8	7.44	6.38 ± 0.89	5.88 ± 0.45	5.69 ± 0.24

Table 6
Companion Frequency and Environment

Category	Number of stars	Number w/companion	Number w/physical companion	Percentage of physical companion
Cluster/association	83	41	31	37 ± 7
Field	9	2	1	11 ± 11
Runaway	24	8	1	4 ± 4

to a background density in the Orion model of $\eta = 1$ star per AEOS FOV. Thus, we adopted this value of η in Equation (4) to identify the probable physical companions among the cluster and association stars.

The background limits for the field and runaway stars depend instead upon on the stellar number density of Galactic background stars as a function of magnitude and the direction of a given target. Here we adopted the cumulative star counts as a function of apparent *I* magnitude and Galactic coordinates from the Besançon model of the Galaxy (Robin et al. 2003). We created a cumulative star counts versus $\triangle I$ relation for each of these stars and found a limiting magnitude for a specified value of 0.01 stars per AEOS FOV. We set this conservative limit based on numerical experiments for the set of runaway stars with observed faint companions. None of these companions can be physical companions since any such wide binary would be disrupted at the time the runaway star was ejected (by close gravitational encounters or a supernova in a binary).

The results of this exercise to discern the probable physical companions are summarized in Table 6. The targets were placed in categories of cluster and association stars, field stars, and runaway stars according to the criteria adopted by Mason et al.

(1998) (with some revisions from the subsequent work on field O-stars by de Wit et al. 2004, 2005). We see that after rejection of the possible background stars there is still a high frequency (37%) of detected companions among the cluster and association stars in our survey. In sharp contrast, there are very few such companions among the field and runaway stars. The only field star with a probable companion is HD 48279, and de Wit et al. (2004) show that this star is 28″ from a cluster identified in 2MASS images, which suggests that this O-star may be a member of a young, emerging cluster. The only runaway star with a candidate companion is HD 34078 = AE Aur, a star ejected from the Orion association (Gualandris et al. 2004). There is another optical companion, SEI 136, at a separation of 8″.4 (Mason et al. 1998), and we suspect that both the companion we found and SEI 136 form a visual system that appears by a chance alignment with AE Aur at this time in its trajectory across the sky.

Our results confirm the trends found by Mason et al. (1998) that binary O-stars are common among O-stars found near their birthplaces and are rare among O-stars ejected from clusters. These trends are consistent with current models for the ejection of runaways and the formation of massive stars (Zinnecker

& Yorke 2007). High-velocity O-stars were probably ejected by close encounters between binaries in dense clusters and by supernova explosions in close binaries (Hoogerwerf et al. 2001), and their ejection velocities generally exceed the escape velocity binding any wide, orbiting companion. Many massive stars are probably born in high-density stellar environments where binaries may be formed through three-body interactions (Bate et al. 2002) and through the interactions with large proto-stellar accretion disks (Moeckel & Bally 2007). Even in lower-density environments, binaries may form through disk fragmentation and subsequent gas accretion (Kratter et al. 2007). Our results add to growing body of evidence that the formation of binaries is closely linked to the formation of massive stars and the deposition of the angular momentum reservoir of the natal cloud.

REFERENCES

Abt, H. A., Levy, S. G., & Gandet, T. L. 1972, AJ, 77, 138
Africano, J. L., Cobb, C. L., Dunham, D. W., Evans, D. S., Fekel, F. C., & Vogt, S. S. 1975, AJ, 80, 689
Bate, M. R., Bonnell, I. A., & Bromm, V. 2002, MNRAS, 336, 705
Boyajian, T. S., et al. 2005, ApJ, 621, 978
Boyajian, T. S., et al. 2007a, PASP, 119, 742
Boyajian, T. S., et al. 2007b, ApJ, 664, 1121
Caballero, J. A. 2007, A&A, 466, 917
Caballero, J. A. 2008, MNRAS, 383, 750
Cox, A. N. 2001, Allen's Astrophysical Quantities (4th ed.; New York: Springer)
Cutri, R. M., et al. 2003, 2MASS All Sky Catalog of Point Sources (Pasadena, CA: NASA/IPAC)
de Wit, W. J., Testi, L., Palla, F., Vanzi, L., & Zinnecker, H. 2004, A&A, 425, 937
de Wit, W. J., Testi, L., Palla, F., & Zinnecker, H. 2005, A&A, 437, 247
Fabricius, C., & Makarov, V. V. 2000, A&A, 356, 141
Fitzpatrick, E. L. 1999, PASP, 111, 63
Gies, D. R., & Bolton, C. T. 1986, ApJS, 61, 419
Gualandris, A., Portegies Zwart, S., & Eggleton, P. P. 2004, MNRAS, 350, 615
Hartkopf, W. I., Mason, B. D., & McAlister, H. A. 1996, AJ, 111, 370

Hartkopf, W. I., Mason, B. D., & Worley, C. E. 2001, AJ, 122, 3472
Hillenbrand, L. A. 1997, AJ, 113, 1733
Hillwig, T. C., Gies, D. R., Bagnuolo, Jr., W. G., Huang, W., McSwain, M. V., & Wingert, D. W. 2006, ApJ, 639, 1069
Hinkley, S., et al. 2007, ApJ, 654, 633
Hoogerwerf, R., de Bruijne, J. H. J., & de Zeeuw, P. T. 2001, A&A, 365, 49
Hopmann, J. 1967, Mitteilungen der Universitaets-Sternwarte Wien, 13, 49
Hummel, C. A., White, N. M., Elias, II, N. M., Hajian, A. R., & Nordgren, T. E. 2000, ApJ, 540, L91
Kratter, K. M., Matzner, C. D., & Krumholz, M. R. 2007, arXiv:0709.4252
Kraus, S., et al. 2007, A&A, 466, 649
Maíz-Apellániz, J., Walborn, N. R., Galué, H. A., & Wei, L. 2004, ApJS, 151, 103
Makidon, R. B., Sivaramakrishnan, A., Perrin, M. D., Roberts, L. C., Jr., Oppenheimer, B. R., Soummer, R., & Graham, J. R. 2005, PASP, 117, 831
Martins, F., Schaerer, D., & Hillier, D. J. 2005, A&A, 436, 1049
Mason, B. D., Hartkopf, W. I., Gies, D. R., Bagnuolo, Jr., W. G., ten Brummelaar, T. A., & McAlister, H. A. 1998, AJ, 115, 821
Mason, B. D., Hartkopf, W. I., Holdenried, E. R., & Rafferty, T. J. 2001a, AJ, 121, 3224
Mason, B. D., Wycoff, G. L., Hartkopf, W. I., Douglass, G. G., & Worley, C. E. 2001b, AJ, 122, 3466
Massey, P., Armandroff, T. E., Pyke, R., Patel, K., & Wilson, C. D. 1995, AJ, 110, 2715
McSwain, M. V. 2003, ApJ, 595, 1124
McSwain, M. V., Boyajian, T. S., Grundstrom, E. D., & Gies, D. R. 2007, ApJ, 655, 473
Mdzinarishvili, T. G., & Chargeishvili, K. B. 2005, A&A, 431, L1
Moeckel, N., & Bally, J. 2007, ApJ, 661, L183
Morrell, N., & Levato, H. 1991, ApJS, 75, 965
Otero, S. A. 2007, Open Eur. J. Variable Stars, 72, 1
Perryman, M. A. C., & ESA 1997, The *Hipparcos* and *Tycho* Catalogues. Astrometric and Photometric Star Catalogues Derived from the ESA *Hipparcos* Space Astrometry Mission, ESA SP Series Vol. 1200 (Noordwijk: ESA Pub. Div.)
Pozzo, M., Jeffries, R. D., Naylor, T., Totten, E. J., Harmer, S., & Kenyon, M. 2000, MNRAS, 313, L23
Rauw, G., et al. 2002, A&A, 394, 993
Roberts, Jr., L. C. 2001, in Proc. 2001 AMOS Technical Conference, ed. P. Kervin, L. Bragg, & S. Ryan (Maui, HI: Maui Econ. Devel. Board), 326
Roberts, Jr., L. C., & Neyman, C. R. 2002, PASP, 114, 1260
Roberts, Jr., L. C., Turner, N. H., & ten Brummelaar, T. A. 2007, AJ, 133, 545
Robin, A. C., Reylé, C., Derrière, S., & Picaud, S. 2003, A&A, 409, 523
Rossiter, R. A. 1955, Publ. Michigan Obs., 11, 1
See, T. J. J. 1898, AJ, 18, 181
Seymour, D. M., Mason, B. D., Hartkopf, W. I., & Wycoff, G. L. 2002, AJ, 123, 1023
Silbernagel, E. 1931, Astron. Nachr., 241, 33
Struve, F. G. W. 1837, Astron. Nachr., 14, 249
ten Brummelaar, T. A., Hartkopf, W. I., McAlister, H. A., Mason, B. D., Roberts, Jr., L. C., & Turner, N. H. 1998, in Proc. SPIE, Adaptive Optical System Technologies, ed. D. Bonaccini, & R. K. Tyson (Bellingham, WA: SPIE), 3353, 391
ten Brummelaar, T. A., Mason, B. D., Bagnuolo, Jr., W. G., Hartkopf, W. I., McAlister, H. A., & Turner, N. H. 1996, AJ, 112, 1180
ten Brummelaar, T. A., Mason, B. D., McAlister, H. A., Roberts, Jr., L. C., Turner, N. H., Hartkopf, W. I., & Bagnuolo, Jr., W. G. 2000, AJ, 119, 2403
van den Bos, W. H. 1928, Ann. Leiden Obs., 14, pt. 4
van Loon, J. T., & Oliveira, J. M. 2003, A&A, 405, L33
Wallenquist, A. 1934, Ann. Bosscha Obs. Lembang, 6, pt. 2
Wegner, W. 1994, MNRAS, 270, 229
Worley, C. E. 1990, in Errors, Bias and Uncertainties in Astronomy, ed. C. Jaschek, & F. Murtagh (Cambridge: Cambridge Univ. Press), 419
Wycoff, G. L., Mason, B. D., & Urban, S. E. 2006, AJ, 132, 50
Zinnecker, H., & Yorke, H. W. 2007, ARA&A, 45, 481